Supporting Information

Bio-inspired synthesis of mesoporous HfO_2 nanoframe as reactors for piezotronic polymerization and Suzuki coupling reactions

*Haiqing Wang, *[a] Dehui Sun, [a] Qichen Lu, [b] Fulei Wang, [c] Lili Zhao, [a]* Zengfu Zhang, [a] *Xun Wang* [b] *and Hong Liu *[ac]*

[a] Institute for Advanced Interdisciplinary Research (iAIR), University of Jinan, Jinan 250022, China.

[b] Key Lab of Organic Optoelectronics and Molecular Engineering, Department of Chemistry, Tsinghua University, Beijing 100084, China

[c] State Key Laboratory of Crystal Materials, Shandong University, Jinan 250100, PR China

Corresponding Authors

* E-mail: ifc_wanghq@ujn.edu.cn

* E-mail: hongliu@sdu.edu.cn

EXPERIMENTAL SECTION

Materials. Dihafnium dichloride (>97.0 wt.%) was purchased from Alfa Aesar. Acetone (AR), ferrocene, hafnium (IV) chloride, ammonia solution (25 wt.%) and aniline (AR) were purchased from Sinopharm Chemical Reagent Co.

Sample Preparation. Synthesis of mesoporous HfO_2 nanoframes (designated as MHFs). A certain amount of dihafnium dichloride (0.1 g) were dissolved in 30 mL acetone with to form a colorless solution. After strong agitation 5 min, 0.5 mL of ammonia was added drop by drop. Then, the obtained mixture was transferred to a 40 ml Teflon-lined stainless steel autoclave. The autoclave was sealed and heated in the oven at 200 ^{o}C for 12 h, and then was cooled down to room temperature naturally. The brown precipitate was recovered using centrifugation at 10000 rpm for 3 min, followed by washing with acetone for several times. The precipitate was finally dried at 60 ^{o}C for 3 h in an air oven. And then the samples were calcined at 500 ^{o}C for 2 h to obtain the resultant crystallized nanoparticle (i.e. MHFs). Synthesis of hollow HfO_2 nanospheres (labeled as HHSs). The synthesis of HHSs was repeated with the same conditions with MHFs except for the utilization of ammonia.

Characterizations. X-ray diffraction (XRD) patterns of the samples were measured on a Bruker D8 Advance X-ray diffractometer using Cu Kα radiation (λ=1.5418 Å). Scanning electron microscopy (SEM) images were acquired with a Hitachi SU8010 Field Emission Gun Scanning Electron Microscope at 5 kV. Transmission electron microscopy (TEM) graphs were observed by using a Hitachi H-7700 TEM operating at 100 kV. High-resolution transmission electron microscopy (HRTEM), dark-field scanning transmission electron microscopy (STEM), as well as energy dispersive X-ray (EDX) element mapping tests were performed on a FEI Tecnai G2 F20 STwin microscope at 200 kV. N_2 adsorption-desorption isotherms were measured on a

Micromeritics ASAP 2010 automatic adsorption instrument at 77 K. Before the measurements, calcined samples were degassed in vacuum at 150 ^oC for 2 h. Surface areas were calculated using the Brunauer-Emmett-Teller (BET) equation. Thermogravimetric (TG) analysis was carried out at a heating rate of 10 °C/min from room temperature to 1000 ^oC under an air atmosphere (Mettler Toledo, TGA/SDTA 851e). Fourier-transform infrared (FT-IR) spectra were recorded on a Perkin Elmer FTIR spectrophotometer in the range of 4000-400 cm^{-1} with a resolution of 4 cm^{-1} using KBr pellet technique. The Raman spectra were recorded by a Horiba JY H-800 Raman spectrometer. Ultraviolet-visible spectrophotometry (UV-vis) absorption spectra were obtained by a Hitachi U-3900 Spectrophotometer. X-ray photoelectron spectroscopy (XPS) signals were collected by a Thermo Fisher ESCALAB 250Xi spectrometer applying monochromatic Al Kα X-ray sources (1486.6 eV) at 2.0 kV and 20 mA. Piezoelectric properties of samples were characterized using a Scanning Probe Microscope (Dimension Icon, Bruker) with an SCM-PIT, Pt-coated conductive tip. To obtain a stable piezoelectric signal from the sample, the powders uniformly dispersed in alcohol were dropped on an Au-coated silicon wafer, and then coated with a 2-3 nm thick Au film.

Pseudo-electrochemical Polymerization. In a typical procedure, the reaction solution was prepared by mixing HCl, H_2SO_4 and deionized water to obtain a total volume of 200 mL with 0.4 M HCl and 0.15 M H_2SO_4. And then the mixture was precooled to 0 °C. 0.09 g of MHFs and a certain amount of aniline (0.8 M) were added into the above solution. The suspension was transferred to ultrasonic cleaner to be treated for 3 h at 40 kHz and 50 W, during which an ice-bath was used to maintain the 0 °C of reaction temperature. The precipitate was collected by centrifugation and washed with deionized water for three times to remove the residual aniline.

Preparation and catalytic test of mesoporous nanoframe reactor. 40 mg sample powder was dispersed in 20 mL water and ultrasonicated for 3 min. 0.24 mL $PdCl_2$ aqueous solution (0.02 M) was added and after being stirred for 10 min, 60 mg $NaBH_4$ was introduced to form Pd nanoparticles. The catalyst powder was collected with centrifugation after a certain time stirring. The classical Suzuki coupling reaction was used as a model to demonstrate the structural advantages in catalysis. The catalysis was started at room temperature by mixing 15 mg catalyst, 10 mL ethanol and 10 mL water, 0.218 g P-iodobenze, 0.15 g phenylboronic acid, and 0.3 g potassium carbonate. The reaction productions at different time points were analyzed exploiting Shimadzu gas chromatography.

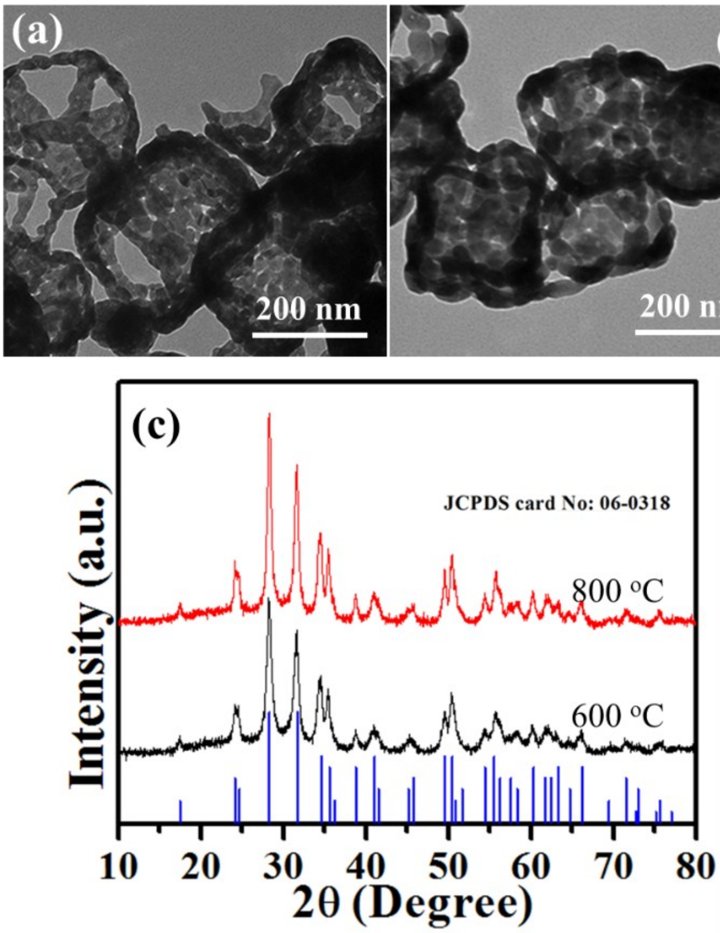

Figure S1 TEM images of MHFs calcined at (a) 650 °C and (b) 800 °C, (c) XRD patterns.

Figure S1 demonstrate that the nanoframes are stable with calcination temperature up to 800 °C for 2 h in air. The results imply excellent solvothermal and thermal stability of mesoporous HfO_2 nanoframes. Therefore, the mesoporous HfO_2 nanoframes can also be much expected for various important catalysis applications in both liquid and gas phases, such as cellulose conversion, methanol synthesis, water-gas-shift reaction, transesterification reaction, hydrodesulfurization, ketonization of carboxylic acids, and so on.[1-4, 5]

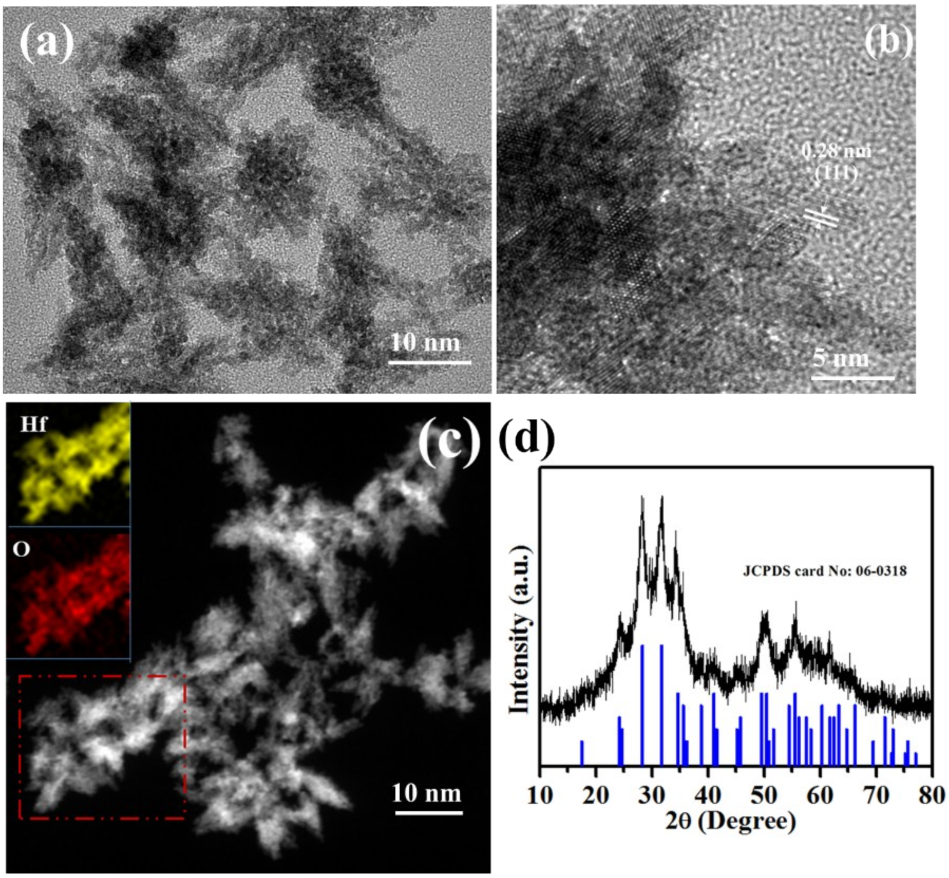

Figure S2 (a) Low-magnification and (b) high-magnification HRTEM images, (c) HAADF-STEM (inset, EDX mapping), (d) XRD pattern of flower-like HfO_2 aggregations.

The HfO_2 aggregations were prepared via the same procedure with hollow sphere but with 30 mg of Hf precursor. Figure S2 shows the lower-like morphology of aggregations. The Hf and O elements are uniformly dispersed throughout the whole aggregations. The XRD pattern (Figure 2Sd) indicated the monoclinic crystalline phase of flower-like HfO_2 aggregations.

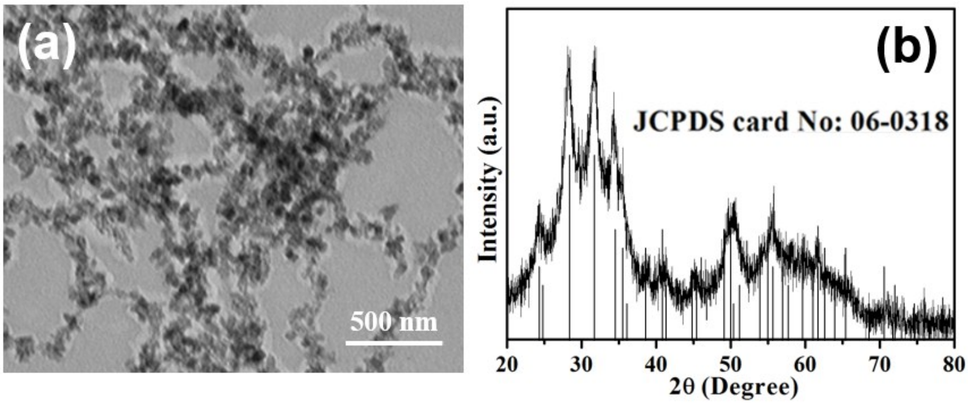

Figure S3 (a) Low-magnification TEM image and (b) XRD pattern of HfO_2 nanoparticles synthesized with $HfCl_4$ as precursor.

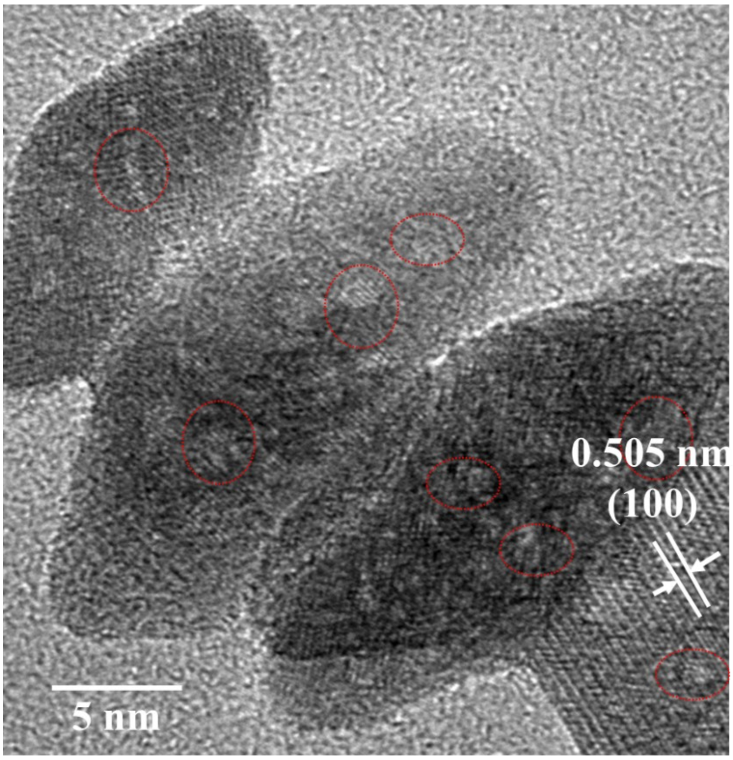

Figure S4 HRTEM image of defect-rich HfO_2 nanoparticles

As for the synthesis of defect-rich nanoparticles, the solvent acetone was replaced with deionized water and no ammonia was used. The defect-rich nanoparticles were prepared by treating the product at 500 ^{o}C for 2 h to remove the organics. As marked with red circles, the discontinuous lattice fringe implies the numerous defects on the surface of the HfO_2 nanoparticles. The reference HfO_2 nanoparticle in manuscript are obtained by calcined the defect-rich nanoparticles at 900 ^{o}C for 2 h in air.

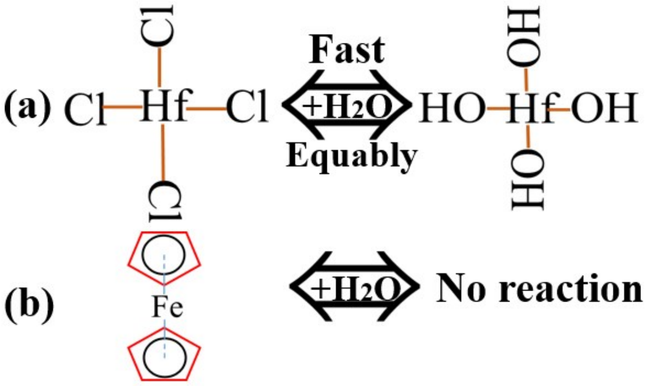

Figure S5 Illustration of the hydrolysis of $HfCl_4$ and Cp_2Fe.

Figure S5 exhibits a general hydrolysis process of $HfCl_4$ and ferrocene. The $HfCl_4$ with chloride ion ligands can be instantaneously hydrolyzed due to the isotropous features, while the bonds between cyclopentadiene ligand and central iron atom in ferrocene are too stable to break at given conditions. As a result, no product was observed for ferrocene as metal precursor. Combined with Figure 3a, the anisotropic and isotropic precursors induced hydrolysis difference can be illustrated for a straightforward understanding to the morphology diversity, which is very similar to the assembly principles in biomolecules.

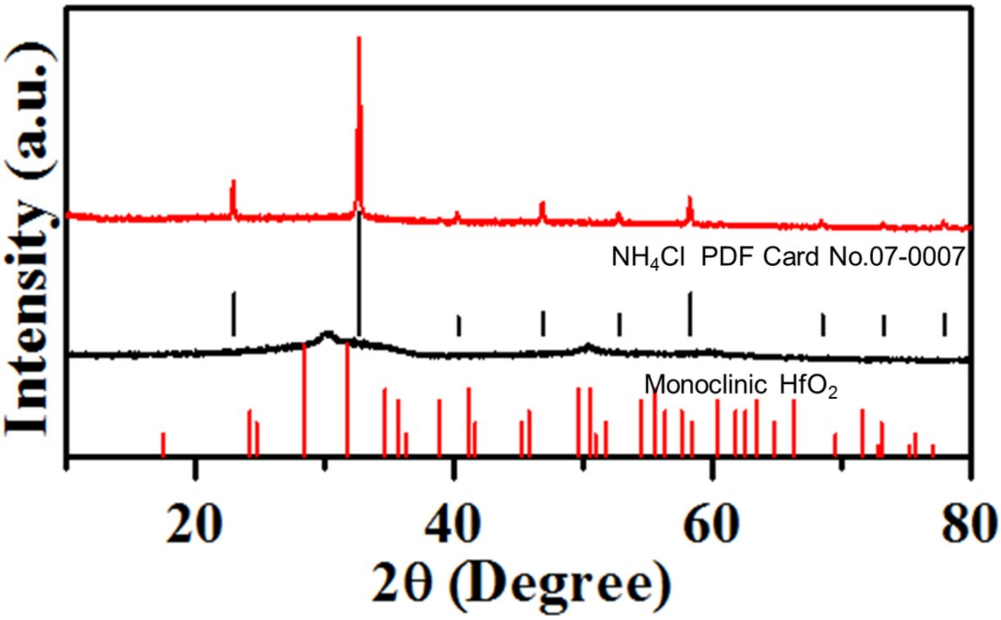

Figure S6 XRD patterns of the intermediate (black) and as-prepared production (red).

The XRD patterns of the reaction precipitation before solvothermal process were collected and shown in Figure S6. The strong XRD peaks (black line) can accord well with the crystalline NH_4Cl and the red line shows amorphous feature implying the disappearance of NH_4Cl after water washing.

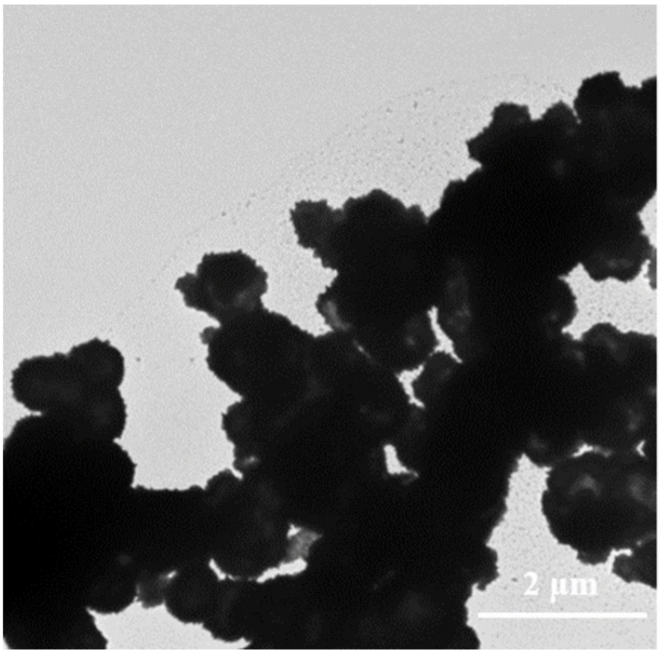

Figure S7 TEM image of the product with NaOH as alkali source.

Figure S7 shows the vague morphology of HfO_2 nanostructures prepared with NaOH replacing ammonia as alkaline source.

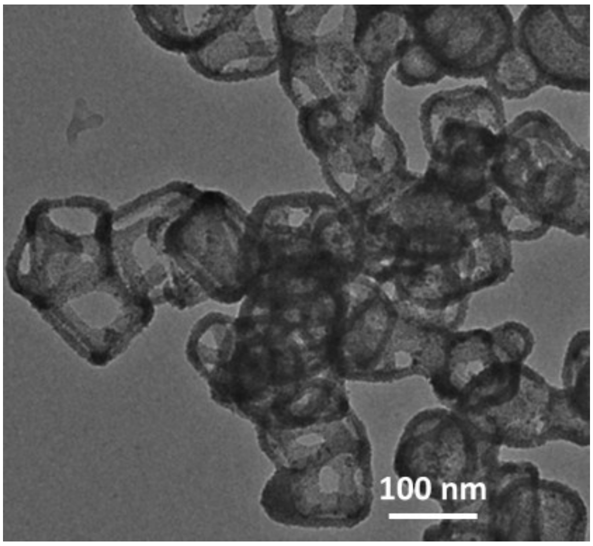

Figure S8 TEM image of nanoframe synthesized with cyclohexane as additive.

In order to demonstrate the flexibility of anisotropic Hf precursor in morphology and size control, the organic cyclohexane was used as additive for the synthesis of nanoframe. Figure S8 indicates a nanoframe with 100 nm of length and ~10 nm thickness of arris, which is smaller than the size of the nanoframe in Figure 1. The result further confirmed the anisotropic Cp_2HfCl_2 is versatile for the morphology and size control.

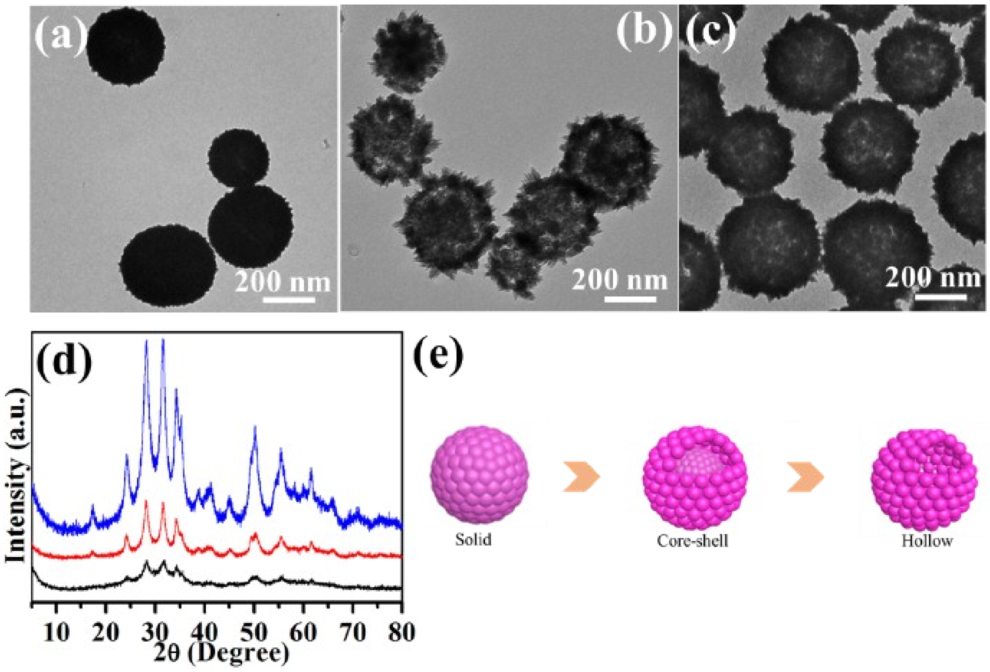

Figure S9 (a, b and c) TEM images of time-dependent products, (d) their corresponding XRD patterns, (e) illustration for the evolution of hollow HfO_2 sphere.

The evolution process of the hollow HfO_2 spheres with different hydrothermal treatment time (4 h of Figure S9a, 8 h of Figure S9b and 12 h of Figure S9c) was tracked with TEM images to investigate the possible formation mechanism. As shown in Figure S9, it was found that the solid spheres with a smooth surface were formed at 4 h. Further prolonging the treatment time to 8 h, the interior of the spheres gradually became empty and the unique urchin-like yolk-shell structures was formed. These cores shrink with time, giving rise to an increased interspace. As a result, the uniform hollow HfO_2 spheres were formed. The XRD peaks are becoming stronger with the prolonging the hydrothermal time (Figure S9d). Obviously, the evolution of hollow nanostructures described here proceeds spontaneously without the removal of micro/nanobeads by harsh oxidizing agents or applied potential involved in the Kirkendall effect[6] and the galvanic displacement methods. The evolution process of hollow HfO_2 spheres should follow a typical the Ostwald ripening process, as illustrated by Figure S9e.

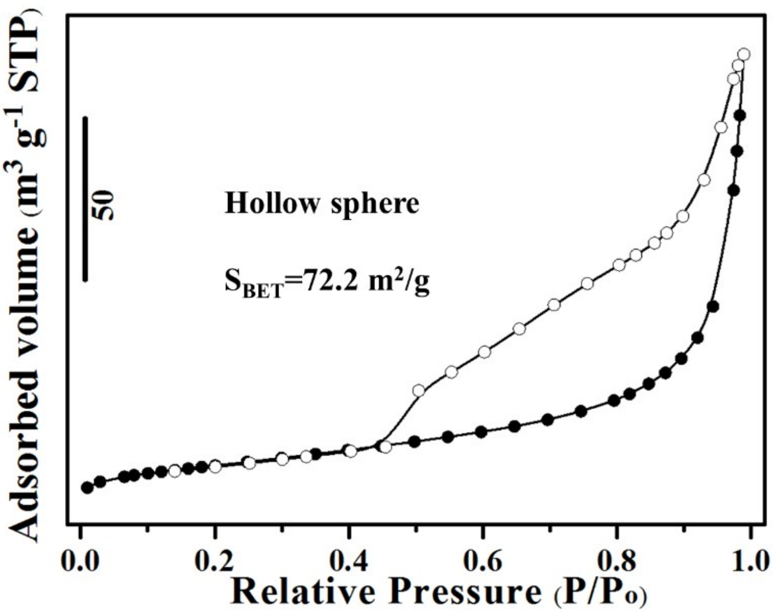

Figure S10 Nitrogen physisorption of HfO_2 hollow spheres

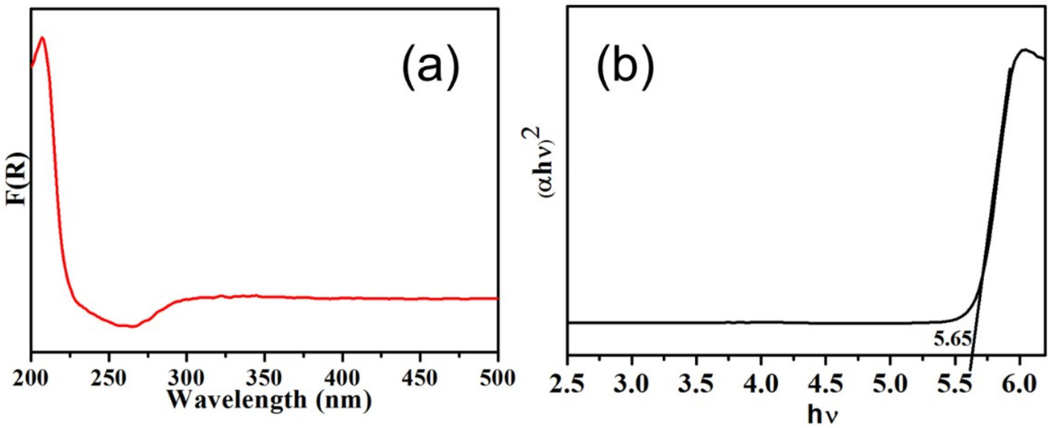

Figure S11 (a) UV-Vis spectrum of MHFs and (b) variation of $(\alpha h\nu)^2$ with photon energy for MHFs.

The energy band gap (E_g) value of calcined HfO_2 MHFs was obtained by absorption spectra and plotting $(\alpha h\nu)^2$ vs photon energy ($h\nu$) using the following relation:

$(\alpha h\nu)^2 = A(h\nu - E_g)$ (1)

where α is the absorption coefficient, A is the constant, and E_g is the band gap of the MHFs, respectively. The value was calculated by extrapolating the linear portion of the curve to ($h\nu$) axis.

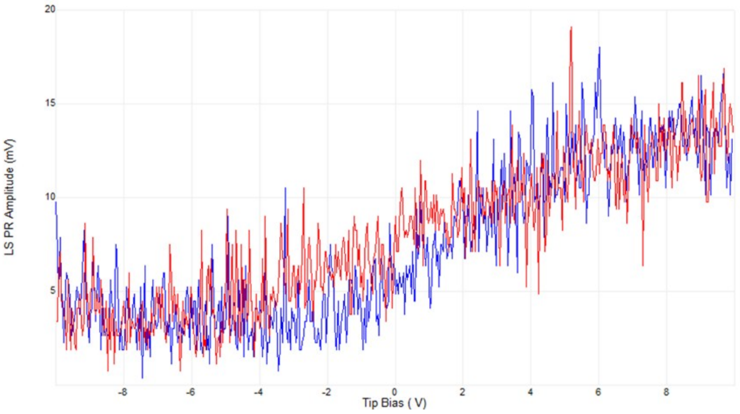

Figure S12 the standard ferroelectric amplitude curve of nanoframe.

The standard ferroelectric butterfly amplitude curve (Figure S12) was obtained. The butterfly amplitude curve shows the apparent variation in the amplitude, which is related to the changing strain under an external field. This is the embodiment of the piezoelectric characteristic

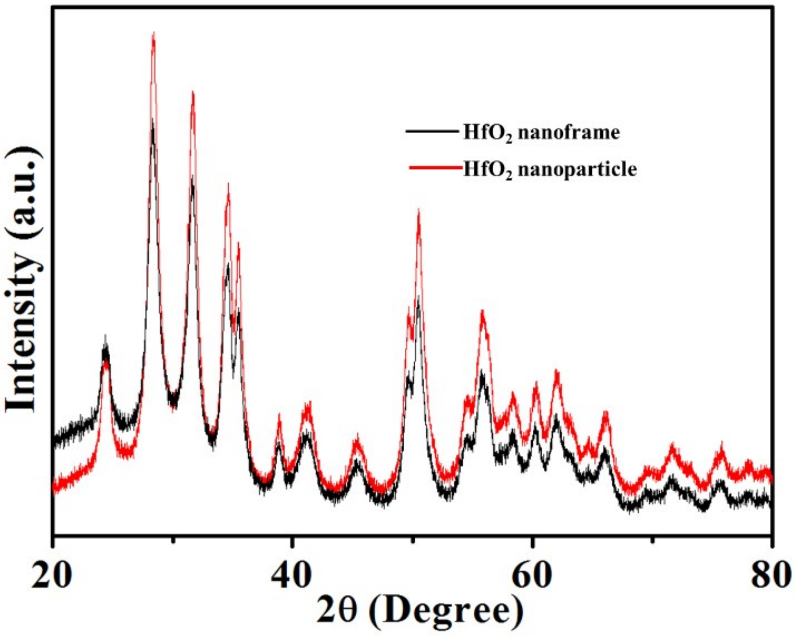

Figure S13 XRD patterns of HfO_2 nanoframe and nanoparticle composites.

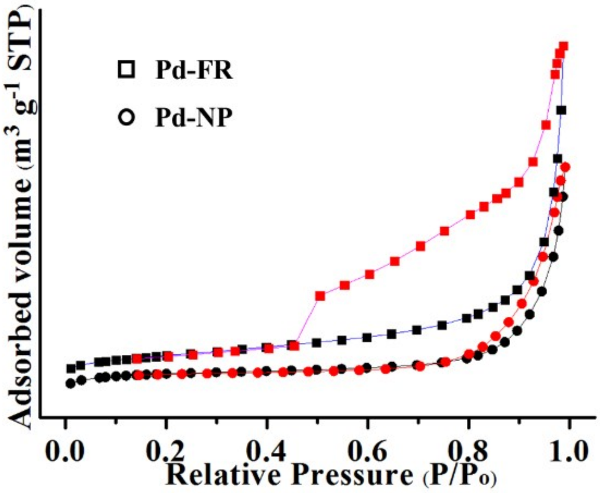

Figure S14 Nitrogen physisorption of Pd-FR and Pd-NP.

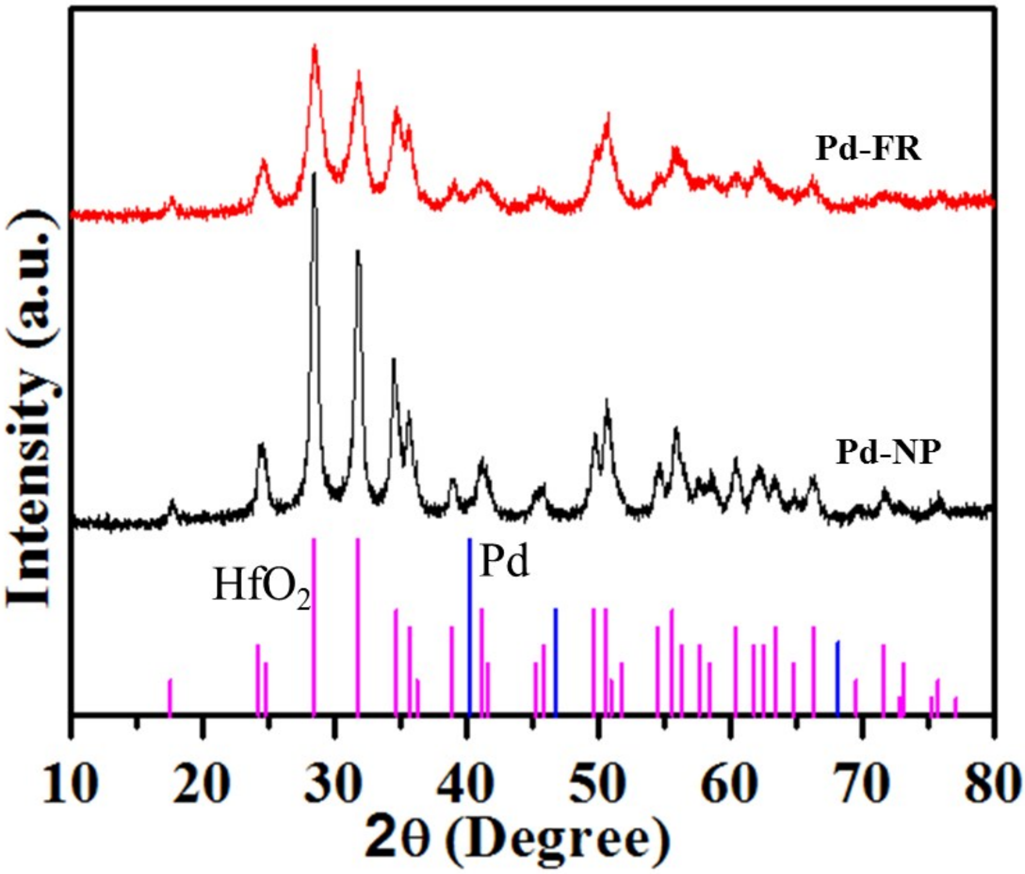

Figure S15 XRD patterns of Pd-FR and Pd-NP (The pink lines (blue lines) index to monoclinic HfO_2 (Pd)).

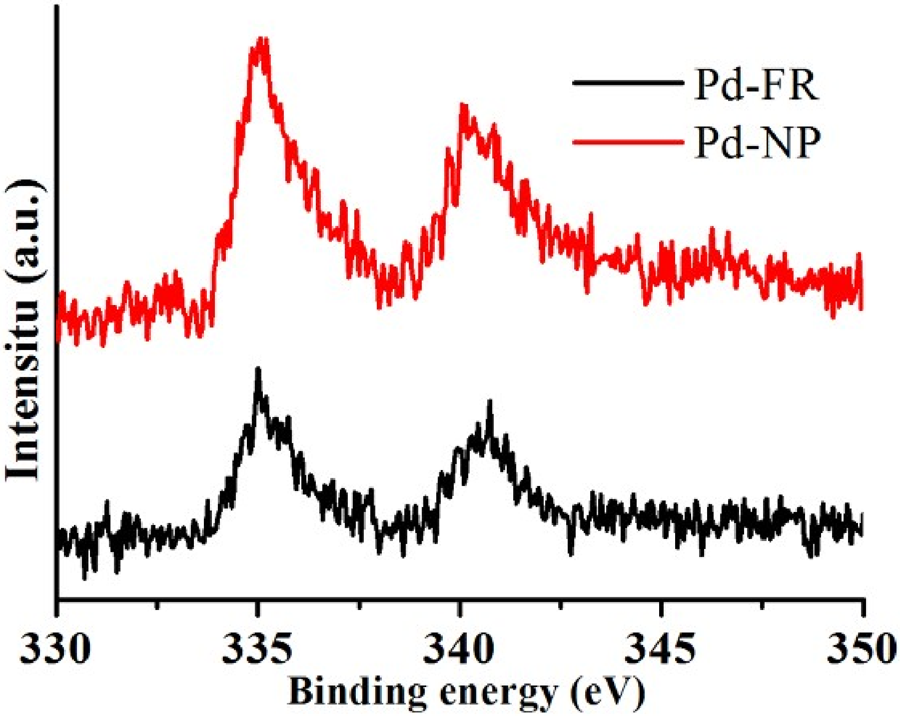

Figure S16 Pd 3d XPS spectra of Pd-FR and Pd-NP.

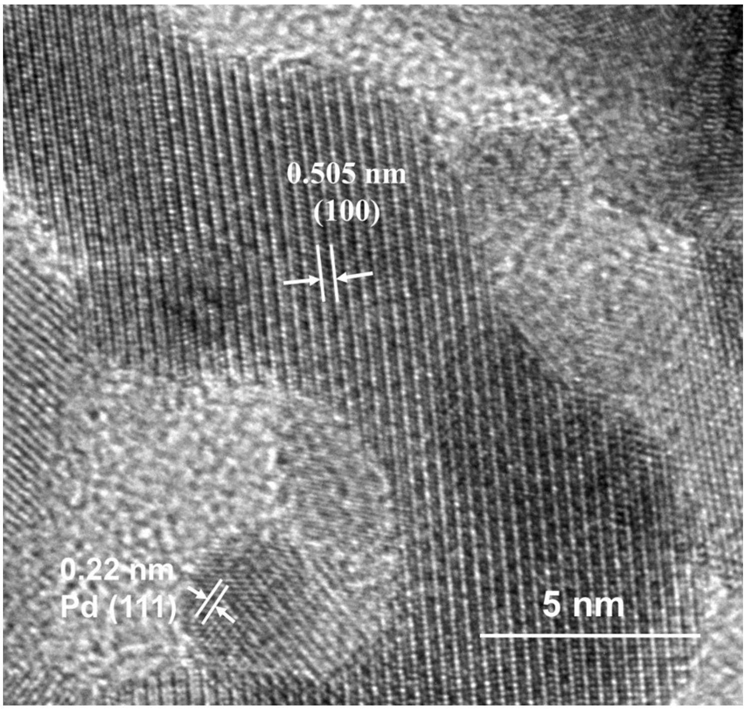

Figure S17 HRTEM image of Pd-HS

References

1. K. Samson, M. Śliwa, R. P. Socha, K. Góra-Marek, D. Mucha, D. Rutkowska-Zbik, J. F. Paul, M. Ruggiero-Mikołajczyk, R. Grabowski and J. Słoczyński, *ACS Catal.* 2014, **4**, 3730.
2. H. Xie, J. Lu, M. Shekhar, J. W. Elam, W. N. Delgass, F. H. Ribeiro, E. Weitz and K. R. Poeppelmeier, *ACS Catal.*, 2013, **3**, 61.
3. M. Ruppert Agnieszka, M. Niewiadomski, J. Grams and W. Kwaphiski, *Appl. Catal. B-Environ.*, 2014, **145**, 85.
4. M. Massa, A. Andersson, E. Finocchio, G. Busca, F. Lenrick and L. R. Wallenberg, *J. Catal.*, 2013, **297**, 93.
5. M. R. Jones, R. J. Macfarlane, B. Lee, J. Zhang, K. L. Young, A. J. Senesi and C. A. Mirkin, *Nat. Mater.*, 2010, **9**, 913.
6. X. Liang, X. Wang, Y. Zhuang, B. Xu, S. Kuang and Y. Li, *J. Am. Chem. Soc.*, 2008, **130**, 2736.